# A Model for the Reduction of Specific Surface Area of Powders with Age

**Problem presented by**

Janella Mansell, Rod Drake and John P. Curtis

*A.W.E. Ltd., Aldermaston, Reading, Berkshire RG7 4PR.*

**Executive Summary**

PETN is a high explosive, sometimes stored for periods of up to many years, in powdered form. In storage, the explosive particles change size and shape owing to sublimation, condensation and surface diffusion. AWE measurements are available on the changing particle size distribution (PSD), and the specific surface area (SSA) of the powder, taken from experiments on accelerated ageing. But a mathematical model of the ageing process is wanted in order to interpret the processes at work. Various modelling issues and unusual features of the measurement data were discussed. Four models of important processes were developed, and are reported here. Model (i) addresses the fundamental physics associated with the transport of mass by sublimation, diffusion and condensation. Model (ii) uses chemical kinetics to develop a system of ordinary differential equations (ODEs) for the time-evolution of the frequencies of particle sizes. Model (iii) extends Model (ii) to a continuum particle size distribution. Lastly, Model (iv) considers the growth of particles as described by Cahn-Hilliard equations for the inter-particle transport of matter in Ostwald Ripening. Models (i) and (iv) include the complex geometry and thermodynamics of the problem. By contrast, Models (ii) and (iii) focus on the time evolution of the PSD, but they are more difficult to associate with controllable variables, such as ambient temperature. Our discussions of models (ii) and (iii) suggest we can choose mass-transfer rate constants that reproduce the kind of observed evolution to a bimodal PSD. But more investigation is needed to determine how the rate constants may be associated with the particles' geometry and the thermodynamics of the mass transport processes.

**Version 0.2**
**July 2, 2012**
iii+24 pages

## Report authors

Mark J. Cooker, Lloyd Chapman, Colm Connaughton, Erhan Coskun,
John P. Curtis, Andrea Fernández, Cameron Hall, Andrew Lacey,
John Ockendon, Tom Ranner.

## Contributors

Jonathan Black (University of Oxford)
Lloyd Chapman (University of Oxford)
Colm Connaughton (University of Warwick)
Mark J. Cooker (University of East Anglia)
Erhan Coskun (Karadeniz Technical University)
Russell Davies (Cardiff University)
Andrea Fernández (Bath University)
Cameron Hall (University of Oxford)
Andrew Lacey (Heriot-Watt University)
John Ockendon (University of Oxford)
Colin Please (University of Southampton)
Tom Ranner (University of Warwick)
Maciej Skorski (Polish Academy of Sciences)
Chang Wang (University of Oxford)

**ESGI85 was jointly organised by**
University of East Anglia, Norwich 16–20 April 2012
The Knowledge Transfer Network for Industrial Mathematics

**and was supported by**
The Engineering and Physical Sciences Research Council

# Contents

**1 Introduction** **1**
1.1 Background and Scope . . . . . 1
1.2 Problem Statement . . . . . 1

**2 Model (i): Fundamental Considerations** **3**
2.1 Fundamentals at Macroscopic Scale . . . . . 3
2.2 Fundamentals at Microscopic Scale . . . . . 4
2.3 Further Considerations of Time Scales . . . . . 4
2.4 Sublimation at Sub-Particle Scale . . . . . 5

**3 Model (ii) Chemical Kinetics ODEs** **6**
3.1 Model Equations . . . . . 6
3.2 Discussion of Model Equations . . . . . 6

**4 Model (iii): Continuum Size Distribution Modelling** **9**
4.1 Discussion of Model Equations . . . . . 9
4.2 Analysis of Continuum Equations . . . . . 11

**5 Model (iv): Cahn-Hilliard Modelling** **12**
5.1 Ostwald Ripening . . . . . 12
5.2 Ripening with Cahn-Hilliard . . . . . 12
5.3 Numerical Treatment and Results . . . . . 14
5.4 Comments on Model (iv) . . . . . 15

**6 Conclusions** **15**
6.1 Points to Take Further . . . . . 15

**7 Bibliographical Note:** **16**

**Bibliography** **16**

# 1 Introduction

## 1.1 Background and Scope

(1.1.1) Explosives powders (e.g. PETN) are prepared at 100 degrees Celsius and undergo early changes in particle size distribution (PSD) and specific surface area (SSA), followed by longer time-scale changes.

(1.1.2) By understanding how these particles behave in situ and interact with neighbours we aim to make a predictive model of the PSD, able to explain the bi-modal (multi-modal) distribution observed in the left-hand plot of Figure 1.

(1.1.3) Experimental and high resolution measurements indicate complex processes, in particular a sharp initial decrease followed by a slower decrease in the SSA of the powder shown in the right-hand plot of Figure 1.

(1.1.4) The modelling aims to predict the influences of material properties and processing temperature on the possible long-term size distributions and the decrease observed in the specific surface area of the powder.

## 1.2 Problem Statement

(1.2.1) This sub-section is the problem statement, as put by AWE Ltd. at the start of the meeting:

Problem Prepared By: Janella Mansell, Rod Drake and John P. Curtis, AWE Aldermaston, Reading, Berkshire RG7 4PR.

**A Model for the Reduction of Specific Surface Area of Powders with Age**

High surface area powders are required in a number of technology areas. For example, the efficiency of catalysts is intimately linked to the surface area of the powder. In our context we are interested in explosives that are in the form of a powder. High surface area, small diameter powders tend to have a high Gibbs surface energy and tend to coarsen to reduce it. The main mechanisms by which powders may change their surface area are believed to be:

1. Evaporation-condensation, in which molecules detach from a particle surface, diffuse through the gas phase, and then condense on the surface of a different particle;

2. surface diffusion, in which the molecule undergoes long-term diffusion on (solid) particle surfaces without detaching into the gas phase.

To date the mathematical modelling of the coarsening process, sometimes referred to as *Ostwald Ripening*, has usually made the assumptions that the explosives comprise a collection of detached spherical particles of differing radii and that mass transfer occurs via the Gibbs-Thompson effect.

While the assumption of spherical shapes is a reasonable starting point, it is known that crystal growth is highly dependent on local surface curvature. It may be that postulation of a distribution of shapes might be a better way to improve the mathematical description of the process. In previous work correction factors are employed to account for particle shapes, surface roughness and the diffusion process. The first highly transient phase of the coarsening process in particular is still not well understood.
The first main aim of the proposed study is to investigate the physical modelling of the atomic-level mass-transfer processes causing coarsening of solid powders, in particular addressing:
A: how to relax the assumption of separate particles, instead allowing contact between them; and
B: under these circumstances how to model evaporation-condensation and surface diffusion.
The next main aim is to model the evolution of the statistical distribution of particles, probably first assuming spherical particles and then relaxing that assumption. If possible it would be good to establish a flexible distribution model which would allow different models of the physical mechanisms to be tested.
AWE will supply a set of references on the physics and chemistry of the atomic mass-transfer processes, and some data on particle distributions and explosive compositions. It is believed that there should be sufficient scope here to engage the academics over the week and to lead to some fruitful academic research. AWE experts will attend full-time to assist with obtaining information and to decide on priorities, etc.

(1.2.2) **Note:** One of the AWE slides, presented at the start of ESGI-85, explained the Gibbs-Thompson effect of evaporation from a spherical particle, the diffusion of the vapour through the inter-particle gas phase and the condensation of vapour onto another spherical particle. (The assumption of spherical particles is contentious.) Let $p_r$ be the equilibrium pressure of a particle of radius $r$, let $p_\infty$ be the equilibrium pressure of the bulk, let $V$ be the volume of molecules in the solid phase, $\sigma$ the surface energy density, $T$ the absolute temperature and $k$ Boltzman's constant. Then an equation for the Gibbs-Thompson effect is said to be

$$kT \ln\left(\frac{p_r}{p_\infty}\right) = \frac{2\sigma V}{r}. \tag{1}$$

Another slide contains expressions that claim to model evaporation and condensation rates as follows. The evaporation mass loss (per unit surface area) during time $\delta t$ (for a spherical particle) is

$$\delta m_- = p_\infty(T) \exp\left(\frac{C}{TR}\right) \sqrt{\frac{M}{2\pi RT}}\, \delta t, \tag{2}$$

where $C$ is a constant which includes the radius of curvature of the particle surface, $M$ is the molecular mass, $R$ is the gas constant, and $P_\infty(T)$ is the

vapour pressure of a large particle. Also the condensation mass gain (per unit area) during time $\delta t$ is:

$$\delta m_+ = p\sqrt{\frac{M}{2\pi RT}}\,\delta t, \tag{3}$$

where $p$ is the background partial pressure.

# 2 Model (i): Fundamental Considerations

## 2.1 Fundamentals at Macroscopic Scale

(2.1.1) Let $\phi$ be the volume fraction of PETN (pentaerythritol tetranitrate) vapour, $\rho_c$ the density of condensate, $\rho_v$ the density of vapour, $D$ the macroscopic mass-transport diffusivity of the vapour and $T$ the absolute temperature. Then mass conservation of PETN implies

$$\frac{\partial}{\partial t}\left((1-\phi)\rho_c + \phi\rho_v\right) = \frac{\partial}{\partial x}\left(D\frac{\partial \rho_v}{\partial x}\right), \tag{4}$$

where $\phi\rho_v$ is relatively small. Heat conservation implies

$$\frac{\partial}{\partial t}\left((1-\phi)c_c\rho_c T + \phi\rho_v(c_p T + L)\right) = \frac{\partial}{\partial x}\left(k\frac{\partial T}{\partial x} + (c_p T + L)D\frac{\partial \rho_v}{\partial x}\right), \tag{5}$$

where $c_c$ and $c_p$ are the specific heat capacities of the solid and vapour, $L$ is the latent heat of vaporisation from solid to vapour, and $k$ is the thermal conductivity. Note that the second and fourth groups of terms in (5) are relatively small. (Equations (4,5) encompass the diffusion of mass and heat, as described by Crank [10].)

(2.1.2) Equations (4, 5) imply the following statement of the Heat Equation.:

$$\rho_c c_c \frac{\partial}{\partial t}\left((1-\phi)T\right) = \frac{\partial}{\partial x}\left(k\frac{\partial T}{\partial x}\right), \tag{6}$$

with an associated time-scale of $\leq 1$ hour. Also we have the Mass Equation.:

$$-\rho_c\frac{\partial \phi}{\partial t} = \frac{\partial}{\partial x}\left(D\frac{\partial \rho_v}{\partial x}\right), \tag{7}$$

where $\rho_v = \rho_v(T)$ changes on a time scale of $6\times10^8$ seconds (20 years), and so we may take $\phi$ to be a constant and model the temperature variation in equation (6) as follows:

$$(1-\phi)\rho_c c_c\frac{\partial T}{\partial t} = \frac{\partial}{\partial x}\left(k\frac{\partial T}{\partial x}\right). \tag{8}$$

## 2.2 Fundamentals at Microscopic Scale

(2.2.1) The time scale for microscopic particle change due to diffusion is $O(\rho_c l_m^2/\rho_v D)$. Here we take $\rho_c = 1.8 \times 10^3\,\mathrm{kg\,m^{-3}}$, length-scale $l_m = 10^{-5}\,\mathrm{m}$, $\rho_v = 1.3 \times 10^{-6}\,\mathrm{kg\,m^{-3}}$ based on a saturation pressure of $1.34 \times 10^{-2}\mathrm{Pa}$ at $T = 350\,K$, and where $D = 10^{-5}\,\mathrm{m^2 s^{-1}}$. Hence the diffusion time scale is found to be $O(10^9 \times 10^5 \times 10^{-10})\mathrm{m^2/m^2\,s^{-1}} = 10^4$ seconds (3 hours).

(2.2.2) In the microscopic problem, with $T$ fixed for the long time scales of interest, the vapour evaporating from a solid particle has a local vapour density whose functional dependence is of the form

$$\rho_v = \rho_s(\phi, k, T, V), \tag{9}$$

in which the vapour flux from the surface is $V = D_v \partial\rho_v/\partial n$, and $n$ is the outward normal distance from the particle's surface, and $D_v$ is the diffusivity of the vapour. Between particles the vapour density diffuses according to the diffusion equation:

$$\frac{\partial \rho_v}{\partial t} = D_v \nabla^2 \rho_v, \tag{10}$$

where $\nabla^2$ is the three-dimensional Laplacian.

(2.2.3) The solutions of equation (10) tend to an equilibrium configuration, that depends on $T$, over a *macroscopic time scale*. However, this mechanism also suggests that a decrease of temperature during an experiment would reverse the downward trend of the SSA.

(2.2.4) N.B. There is an issue over whether the *typical shape* (if such a thing exists) is uniquely matched to each temperature $T$. To get (10) to give a temperature-dependent final particle distribution, the local equilibrium saturation vapour pressure must be given. e.g. by some law of the form (9). Without detailed knowledge of such dependency, we're not in a position to predict the ultimate SSA (specific surface area).

## 2.3 Further Considerations of Time Scales

(2.3.1) For the length scale of the powder particles (and their separation distance), it may be that the mass diffusion would be about 70 (give or take a factor of three or more) times as fast as the porous flow.

(2.3.2) Although temperature diffusion acts on the right time scale for the fast change, it doesn't really explain the fast change of **particle size**. We might postulate the existence of much finer particles, or a much finer structure, which are/is eliminated by the mechanism above (that a shorter length scale leads to a faster time to act).

(2.3.3) In changing the temperature from 350K to 375K, the saturation pressure increases by a factor of about 20. Unfortunately, the experimental results don't appear to show any corresponding reduction of time scale.

(2.3.4) Looking at AWE's two sets of graphs ((1) of size distributions and (2) of SSAs – See Figure 1) we have the following. In (1), the first bump of the "bi-modal" distribution, given the sizes involved, looks as though it contains less than 1% of the mass of the crystals (perhaps more like 0.15%). (There are also suspicions of lower humps to the right – making the distribution at least tri-modal – which could contain more mass, given the relevant length scales, than the more pronounced left-hand bump.) In the first 30 minutes, (1) shows a shift to the right of the main hump, corresponding to a doubling of the particle size. Graph (2) of Figure 1 only indicates a reduction of about 20% (not 50%) in SSA during that period.

## 2.4 Sublimation at Sub-Particle Scale

(2.4.1) Consider a half-space $x > 0$ sublimating happily and steadily over a time scale of days. An isothermal model might be:

$$u\frac{dp}{dx} = D\frac{d^2p}{dx^2}, \qquad \rho u\frac{du}{dx} = -\frac{dp}{dx}, \qquad p = (RT)\rho = \text{constant} \times \rho, \quad (11)$$

where $D$ = diffusion coefficient of PETN in air at absolute temperature $T$. Also we have two boundary conditions at $x = 0$ as follows: $p = p_s$ and $\rho u = -\tilde{D}\frac{dp}{dx}$ (from AWE book [12] or [14]), and a third condition at $x = \infty$ where $p = p_\infty < p_s$.

(2.4.2) Setting $RT = D = 1$ for simplicity, $\frac{1}{2}u^2 + \log\rho = \frac{1}{2}{u_0}^2 + \log\rho_0$.
So

$$\frac{dp}{dx} - \frac{dp}{dx}(0) = -\int_{\rho_0}^{\rho} \sqrt{{u_0}^2 + 2\log\left(\frac{\rho_0}{\rho'}\right)}\,\mathrm{d}\rho', \quad (12)$$

where $p = \rho$ and $\rho_0 = p_s$. Hence we have an o.d.e. for $\rho = p$ of the form:

$$\frac{dp}{dx} = F(p, u_0, p_s), \quad (13)$$

with $p = p_s$ at $x = 0$, and $p = p_\infty$ at $x = \infty$ as boundary conditions which should give sublimation velocity $u_0$ as a function of $p_s$.

(2.4.3) If this is OK maybe we could fit a 10-hour timescale when we put $\frac{\partial p}{\partial t}$ into the mass conservation equation and a half-hour timescale when we consider heat conduction?

# 3 Model (ii) Chemical Kinetics ODEs

## 3.1 Model Equations

(3.1.1) We consider a closed container of fixed volume containing particles of various sizes. We define $c_k(t)$ to be the frequency of those particles that contain $k$ atoms (or have volume $k$), at time $t$, where $t \geq 0$. Therefore $c_1(t)$ is the frequency of monomers, i.e. the vapour.

(3.1.2) Particles can only change size by exchanging monomers via the vapour. Condensation and evaporation mass exchanges are accounted for in the following reaction equations:

$$(k) \oplus (1) \to (k+1) \qquad \text{gain at rate } \gamma_k\, c_k\, c_1 \tag{14}$$

$$(k) \to (k-1) \oplus (1) \qquad \text{loss at rate } \lambda_k\, c_k, \tag{15}$$

where for a particle of volume $k$ its rate of volume decrease by evaporation is at a rate of loss $\lambda_k$, and its volume increase by condensation from the vapour is at a rate of gain $\gamma_k$. Note that both $\lambda_k \geq 0$ and $\gamma_k \geq 0$.

(3.1.3) The following are mean-field equations for a homogeneous mix of particles:

$$\frac{dc_k}{dt} = \gamma_{k-1}c_{k-1}c_1 - \gamma_k c_k c_1 + \lambda_{k+1}c_{k+1} - \lambda_k c_k \quad \text{for} \quad k = 2, ..., N \tag{16}$$

$$\frac{dc_1}{dt} = -2\gamma_1 c_1^2 - c_1 \sum_{k=2}^{N-1} \gamma_k c_k + 2\lambda_2 c_2 + \sum_{k=3}^{N} \lambda_k c_k. \tag{17}$$

## 3.2 Discussion of Model Equations

(3.2.1) A particle of size $k = 1$ is referred to as a monomer, and such particles do not themselves evaporate, so $\lambda_1$ is absent from equations (16, 17). Equation (16) follows from considering the four ways that particles of size $k$ can be made or lost. The terms in turn correspond to: a gain due to a $k-1$ combining with a monomer; a loss when a $k$ loses a monomer by precipitation; the gain of a $k$ because a $k+1$ evaporates a monomer; the loss of a $k$ by evaporation. In (17) the terms on the RHS correspond to the four ways one gains or loses monomers: First, when a pair of monomers combine to form a dimer, there is a loss of *two* monomers. Secondly each $k \geq 2$ particle can combine with a monomer. Thirdly, evaporation of one dimer leads to the making of *two* monomers. Fourthly, any $k \geq 3$ particle can evaporate to make exactly one monomer.

(3.2.2) The equation system (16, 17) is truncated at size $k = N \geq 3$. We artificially stop growth due to condensation from size $N$ to $N+1$, by setting $\gamma_N = 0$, and this is already incorporated into the upper limit of the first

summation in equation (17). Also larger particles are unavailable to evaporate down to size $N$, so we set $\lambda_{N+1} = 0$. Hence the model has a set of $2N-2$ constants, all $\geq 0$: namely $\lambda_2, ..., \lambda_N, \gamma_1, ...., \gamma_{N-1}$.

(3.2.3) A property of equations (16, 17) is conservation of total volume of material:

$$\frac{d}{dt} \sum_{k=1}^{N} k\, c_k = 0, \tag{18}$$

and therefore a fixed total volume, which we can write as a total mass $M$ divided by a constant mean density $\varrho$:

$$\sum_{k=1}^{N} k\, c_k = \frac{M}{\varrho}. \tag{19}$$

(3.2.4) **Forward problem:** Given the rates $\gamma_k$ and $\lambda_k$ we can integrate the rate equations (16, 17) forward in time, until either an equilibrium state is reached or not. If the resulting particle size distribution is similar to the observed data, then the problem is 'solved'.

(3.2.5) For most choices of $\gamma_k$ and $\lambda_k$, the equilibrium state consists of a set of special values $c_k = c_k^*$ which are independent of time. We expect $c_k^*$ to have a monotonically decreasing dependence on $k$. Can we find a set of rate constants $\gamma_k$ and $\lambda_k$ which re-produce a bi-modal (or multi-modal) size distribution in the equilibrium state $\{c_k^*\}$?

(3.2.6) **Inverse problem:** For a **given** observed equilibrium size distribution, $\{c_k^*\}$, we set all the derivatives equal to zero and solve (16, 17) for that set of rates, $\gamma_k$ and $\lambda_k$, which produce the observed $\{c_k^*\}$ equilibrium state, and the problem is again 'solved'. However, how should we choose the constants?

(3.2.7) If $\{c_k^*\}$ is a known equilibrium state, then equations (16, 17) have zero left-hand sides, and can be treated as a set of algebraic conditions to determine the rates $\gamma_k$ and $\lambda_k$. As such, these are LINEAR equations ... but they are under-determined. The under-determination comes from the fact that we have only $N$ independent equations, consisting of just $N-1$ independent conditions from eqs (16, 17) and one inhomogeneous condition from (19). And yet we have $2N-2$ unknown rate constants to find, and, since $N \geq 3$, in general $N < 2N-2$. So we have more unknowns than equations. In principle we can deal with this under-determinedness via Tikhonov regularisation... ... or cheat as follows. Assume $\gamma_k$ are known, or better equal to one unknown value. Then we are left with $N$ equations for $N$ unknowns (e.g. $N-1$ values for $\lambda_k$ plus 1 shared unknown value for all the $\gamma_k$). We must also be mindful of equation (19) when choosing the set of values $c_k^*$.

(3.2.8) Can we find (positive) rates which give a *bimodal* equilibrium PSD? We constructed one example computed with $N = 100$ started with initially uni-modal PSD data. See Figure 2. Solving the forward problem, the PSD evolved over time to a bimodal distribution. The computed long-time distribution sits on top of the independently obtained equilibrium profile, as shown in Figure 2.

(3.2.9) Results were obtained for the inverse problem, to obtain $\lambda_k$, in which we put $\gamma_k = 1$, (i.e. the condensation rates were assumed to have no dependence on particle size – further thought will be needed to determine if this is realistic). These rates $\lambda_k$, obtained from the equilibrium state, are shown in Figure 3. With this input we then solved the forward problem with these inferred rates. With the rates obtained from the inverse problem, do the forward dynamics work to produce a bimodal distribution? We had some success in answering this.

(3.2.10) We also reported on the associated time-evolution of the Specific Surface Area, $SSA$, defined by

$$SSA(t) = \sum_{k=1}^{N} \alpha k^{\frac{2}{3}} c_k(t), \tag{20}$$

where $\alpha$ is a dimensionless shape coefficient. Note that $\alpha$ is independent of $k$ when the particles are dispersed and all share the same shape. It is for spheres that $\alpha$ takes its smallest value: $\alpha = (4\pi)(4\pi/3)^{-2/3} = 4.84$; for cubes $\alpha = 6$. The value of $\alpha$ is larger for the other Platonic polyhedra, up to $\alpha = 7.21$ for regular tetrahedra; still higher values of $\alpha$ occur for stellated or highly crenellated shapes.

(3.2.11) It was found there is a sharp decrease in $SSA(t)$ over a short initial period, followed by a slower decline (to an equilibrium value), similar to the measured behaviour reported in the problem presented. See the example shown in Figure 4, and compare with Figure 1 (right).

(3.2.12) In the equilibrium state (e.g. within a closed environment after a long time) the left-hand sides of equations (16, 17) are zero but, as in the real physical system, the equilibrium is dynamic in that there is a continual exchange of mass between the particles mediated by the monomers of frequency $c_1$.

(3.2.13) **Equilibrium Uniqueness:** Some thoughts on the uniqueness of the equilibrium state $\{c_k^*\}$ are as follows. If the rates $\lambda_k$ and $\gamma_k$ are all known, then we can express the unknowns $c_2^*, ..., c_N^*$ from the $N$ independent equations (16, 19) to obtain one $N^{\text{th}}$ degree polynomial condition on $c_1^*$, which we write as $P_N(c_1^*) = 0$. Although there are $N$ solutions, evidence from $N = 2, 3, 4$ suggests that we can use Descartes' rule of signs on $P_N$, to

show that there is just one real positive root, and the polynomial guarantees the root is (sensibly) such that $c_1^* : 0 < c_k^* < M/\varrho$. (All the other roots are unphysical in that they are negative or complex.) For the rest of the solution set, each $c_k^*$ equals a positive constant times $(c_1^*)^k$. So there is just one positive value of $c_k^*$ for $k = 2, ..., N$. We conclude that the only physically possible equilibrium state may well be unique.

(3.2.14) A particle-size-dependent evaporation loss rate might be modelled by

$$\lambda_k = k([k-60]^2 + 1), \quad \gamma_{k-1} = 100, \; k = 2, \ldots, M, \quad \gamma_M = 0. \tag{21}$$

# 4 Model (iii): Continuum Size Distribution Modelling

## 4.1 Discussion of Model Equations

(4.1.1) In practical problems, we are concerned with mass transfer between very large particles, where $k \approx 10^4$ or greater [21]. (If the dynamical system (16) and (18) were composed of 10,000 variables then it would be too big to treat computationally in practice.) Hence, it is desirable to develop a continuum analogue of the discrete system of differential equations given by (16) and (18) in the previous Model (ii).

(4.1.2) One way of doing this is to assume that $k$ varies naturally on a scale of $\epsilon^{-1}$, so that $\gamma_k$, $\lambda_k$ and $c_k(t)$ are well approximated by smooth functions of a rescaled size variable, $\xi \sim \epsilon\, k$.

(4.1.3) Noting that we may need to rescale our variables, we make the *ansätzë* that

$$\gamma_k = \hat{\gamma}\, \gamma(\xi), \qquad k = 2, 3, \ldots \tag{22}$$

$$\lambda_k = \hat{\lambda}\, \lambda(\xi), \qquad k = 2, 3, \ldots \tag{23}$$

$$c_k(t) = \hat{c}\, c(\xi, \tau), \qquad k = 2, 3, \ldots \tag{24}$$

$$c_1(t) = \hat{m}\, m(\tau), \tag{25}$$

where $\xi = (k-2)\,\epsilon$; $\tau = \hat{t}^{-1}\, t$; and $\hat{\gamma}$, $\hat{\lambda}$, $\hat{c}$ and $\hat{m}$ are all scaling factors chosen so that $\gamma(\xi)$, $\lambda(\xi)$, $c(\xi, t)$ and $m(t)$ are all $\mathcal{O}(1)$ functions. Note that $\hat{\lambda}$ and $\hat{\gamma}$ should be chosen based on the expressions used for $\lambda_k$ and $\gamma_k$, but that $\hat{t}$, $\hat{c}$ and $\hat{m}$ may depend on $\epsilon$, $\hat{\lambda}$, $\hat{\gamma}$ and the other parameters in the model.

(4.1.4) In the following the word 'concentration' is more appropriate than 'frequency' as used in Model (ii) above. In this new model, the monomer concentration, $m(t)$, is treated separately from the concentration of larger particles, and $\xi$ is defined so that $\xi = 0$ corresponds to $k = 2$ (the smallest particles that are not monomers).

(4.1.5) First, applying the Euler-Maclaurin summation formula means that (19) becomes

$$\frac{\hat{m}\,\varrho}{M}\,m(\tau) + \frac{\hat{c}\,\varrho}{\epsilon^2\,M}\int_0^\infty \xi\,c(\xi,\,\tau)\,d\xi + \mathcal{O}\left(\frac{\hat{c}\,\varrho}{\epsilon\,M}\right) = 1.$$

Since most of the mass will be stored in the large particles, it follows that an appropriate nondimensionalisation for concentration is $\hat{c} = \frac{\epsilon^2 M}{\varrho}$.

(4.1.6) To obtain a continuum model, we substitute equations (22) to (25) into (16), and use Taylor series to approximate $c_{k\pm1}$ in terms of $c(\xi,\,t)$ and so on. Assuming that a regular perturbation expansion is valid everywhere, we find that (16) becomes

$$\begin{aligned}\frac{\partial c}{\partial \tau} = \epsilon\,\hat{\lambda}\,\hat{t}\,\frac{\partial}{\partial \xi}\left[\lambda(\xi)\,c(\xi,\,\tau) - \frac{\hat{\gamma}\,\hat{m}}{\hat{\lambda}}\,m(\tau)\,c(\xi,\,\tau)\,\gamma(\xi)\right] \\ + \frac{\epsilon^2\,\hat{\lambda}\,\hat{t}}{2}\,\frac{\partial^2}{\partial\,\xi^2}\left[\lambda(\xi)\,c(\xi,\,\tau) + \frac{\hat{\gamma}\,\hat{m}}{\hat{\lambda}}\,m(\tau)\,c(\xi,\,\tau)\,\gamma(\xi)\right] + \ldots\end{aligned}$$

It follows that the time nondimensionalisation needs to be chosen so that $\hat{t} = \frac{1}{\epsilon\,\hat{\lambda}}$ and the monomer nondimensionalisation must chosen so that $\hat{m} = \frac{\hat{\lambda}}{\hat{\gamma}}$. Hence,

$$\begin{aligned}\frac{\partial c}{\partial \tau} + \frac{\partial}{\partial \xi}\big[\,(\gamma(\xi)\,m(t) - \lambda(\xi))\;c(\xi,\,\tau)\big] \\ - \epsilon\,\frac{\partial^2}{\partial\,\xi^2}\big[\,(\gamma(\xi)\,m(t) - \lambda(\xi))\;c(\xi,\,\tau)\big] = \mathcal{O}\left(\epsilon^2\right). \quad (26)\end{aligned}$$

(4.1.7) At leading order in $\epsilon$, we see that $c(\xi,\,\tau)$ satisfies an advection equation, where the 'velocity' (of transport) is given by $\gamma\,m - \lambda$. Consistent with physical expectations, we find that the particles tend to grow if there is sufficient monomer to make $\gamma\,m - \lambda$ positive, while the particles shrink if $\gamma\,m - \lambda$ is negative.

(4.1.8) In order to obtain an equation for $m(t)$ and a boundary condition for (26), we need to consider the behaviour of small-sized particles. Importantly, there will be a significant difference between the case where $\hat{m} \sim \hat{c}$ and the case where $\hat{m} \gg \hat{c}$. In the latter case, we expect to find a system of discrete equations that need to be solved in the boundary layer region where $k = \mathcal{O}(1)$ and $\xi = \mathcal{O}(\epsilon)$. We did not analyse this situation during the study group; instead we focus on the simpler case, $\hat{m} = \hat{c}$.

(4.1.9) In this case, substituting (22) to (25) into (16) for $k = 2$ yields the result

$$m(t) = c(0,\,t) + \mathcal{O}(\epsilon).$$

(4.1.10) Moreover, substituting into (17) and applying Euler-Maclaurin summation, we find that

$$\frac{\mathrm{d}m}{\mathrm{d}\tau} = \epsilon^{-2} \int_0^\infty \big(\lambda(\xi) - \gamma(\xi)\, m(\tau)\big)\, c(\xi,\tau)\, d\xi + \mathcal{O}\big(\epsilon^{-1}\big).$$

Hence

$$c(0,\,\tau) \approx m(\tau) = \frac{\int_0^\infty \lambda(\xi)\, c(\xi,\,\tau)\,\mathrm{d}\xi}{\int_0^\infty \gamma(\xi)\, c(\xi,\,\tau)\,\mathrm{d}\xi} + \mathcal{O}(\epsilon). \tag{27}$$

(4.1.11) The presence of the diffusive term in (26) means that we also need boundary conditions as $\xi \to \infty$. It seems appropriate to choose $c(\xi,\,\tau) \to 0$ as $\xi \to \infty$, because we do not expect to lose mass to particles of increasing size.

(4.1.12) In future work it would be a good idea to investigate carefully the case where $\hat{m} \gg \hat{c}$; that is, where the number density of monomers is much greater than the number density of larger particles. Intuitively, this seems to be a realistic parameter regime, but it would require careful analysis because of the boundary layer near $\xi = 0$.

## 4.2 Analysis of Continuum Equations

(4.2.1) This continuum model defined by (26) and (27) has dynamics which are surprisingly rich. As noted before, ignoring the $\mathcal{O}(\epsilon)$ terms in (26) yields an advection equation that has characteristic curves, in the $(\xi,\,\tau)$ plane, given by

$$\frac{d\xi}{d\tau} = \gamma(\xi)\, m(\tau) - \lambda(\xi). \tag{28}$$

If $[\gamma\, m - \lambda] > 0$, then particle-growth dominates and the mass is advected (in $\xi$ space) from smaller towards larger particles.

(4.2.2) At equilibrium there are two possibilities for each value of $\xi$:

$$\gamma(\xi)\, m - \lambda(\xi) = 0, \quad \text{or} \quad c(\xi) = 0. \tag{29}$$

For given functions $\gamma(x)$ and $\lambda(x)$, and given $m$, we find that all of the mass accumulates at the values of $\xi$ where both $\gamma(\xi)\, m - \lambda(\xi) = 0$ and $\gamma'(\xi)\, m - \lambda'(\xi) < 0$. However, these conditions are problematic, because of the condition that $c(0) = m$. It is only possible to have mass accumulating at a positive value of $\xi$, if $m$ (and hence $c(0)$) is nonzero, but this is only possible in a very limited range of situations.

(4.2.3) This problem can be regularised by incorporating the small diffusion term in (26). In theory, this will enable us to find reasonable equilibrium solutions, but this analysis still needs to be done. It may also be necessary to perform a detailed analysis of the behaviour of the solution when $k = \mathcal{O}(1)$, in order to find the equilibrium concentrations of the smaller species.

(4.2.4) Interestingly, the structure of the hyperbolic advection equation (obtained from ignoring the diffusion terms in (26)) suggests a way in which we can obtain a bimodal particle size distribution. As long as there are multiple points were $\gamma(\xi)\, m - \lambda(\xi) = 0$ and $\gamma'(\xi)\, m - \lambda'(\xi) < 0$, we expect there to be multiple modes in our final solution. If, for example, $\gamma(\xi)$ is constant, but $\lambda(\xi)$ goes up, down, and then up, it is possible for mass to accumulate at more than one particle size.

# 5 Model (iv): Cahn-Hilliard Modelling

## 5.1 Ostwald Ripening

(5.1.1) The ratio of surface area to volume is smaller for larger spheres, as can be easily seen for a sphere of radius $r$, where the ratio is $3r^{-1}$. On the other hand, it is known that the molecules on the surface of particles are less stable than the ones inside, which implies that larger spherical powders have a higher proportion of stable molecules. Thus larger-particle powders are energetically favourable, as they consist mostly of stable molecules with lower energy. As a result, the molecules on smaller particles prefer to move onto larger ones to reduce the energy of the whole system. This causes the growth of larger particles at the expense of smaller ones – a phenomenon known as Ostwald Ripening. An everyday example is the precipitation of drops from clouds [25].

(5.1.2) When a binary system goes through a certain reaction, the minority component condenses or diffuses onto larger particles. The particles on average grow in radius $\overline{R}(t)$ according to

$$\overline{R}(t)^3 - \overline{R}(0)^3 = Kt, \tag{30}$$

where the constant $K$ depends on the system state variables and parameters, and $t$ is the time variable [31]. This is the main result of LSW theory (Lifshitz, Slyozov, and Wagner) [20], [29].

## 5.2 Ripening with Cahn-Hilliard

(5.2.1) We consider the total energy of the binary system:

$$E_\epsilon(c) = \int_\Omega \left( f(c(x,t)) + \frac{\epsilon}{2} |\nabla c(x,t)|^2 \right) \mathrm{d}x, \tag{31}$$

where $c(x,t)$ is the phase function; $f{:}R \to R$ is a non-negative double-well potential with two minima at $c = c_a, c = c_b$ which are the prefered states of $c$; $\Omega$ is the domain containing the mixture; and $\nabla$ is the gradient operator (in one space dimension $\nabla = \partial/\partial x$). Also $\epsilon$ is a small positive

dimensionless number: the larger the value of $\epsilon$, the sooner ripening takes place. The phase field variable, $c$, describes the state of the system: in the two pure phases (solid and vapour) $c$ takes one of the extreme values, $\pm 1$. The system will seek its equilibrium by minimizing the energy $E_\epsilon(c)$, while keeping the mass $\int_\Omega c(x,t)\mathrm{d}x$ constant, as we assume nothing travels into or out of the container, $\Omega$. The function $c(x,t)$ then has to evolve in the direction opposite to the gradient of $E_\epsilon(c)$. The question is: What is the most appropriate Hilbert space where the gradient results in a convenient local model? This question has been addressed in [9], where it was found that the gradient flow

$$c_t = -D\nabla E_\epsilon(c) \tag{32}$$

results in the following well studied Cahn-Hillard model:

$$c_t = -D(\epsilon\nabla^4 c - \nabla^2 f'(c)), \qquad \text{for} \quad (x,t) \ \text{ in } \ \Omega \times (0,\infty) \tag{33}$$

subject to the boundary conditions

$$\partial_n c = \partial_n \nabla^2 c = 0, \qquad \text{for} \ \ (x,t)\text{in} \ \ \partial\Omega \times (0,\infty) \tag{34}$$

when the gradient is computed over the space $H_0^{-1}$ : zero-averaged subspace of dual space $H_1(\Omega)^*$. In (34) $\partial_n$ represents the derivative along the outward normal direction. Furthermore, the model requires an initial condition $c(x,0) = c_0(x)$.

(5.2.2) For a numerical study and properties of (33)-(34), we refer to [8],[13]. The Cahn-Hilliard model has also been used to simulate particle growth and Ostwald Ripening [19] in Al-In system with a logarithmic potential function $f$ in equation (38) below.

(5.2.3) The original papers on this work, from 1958-59, are by Cahn and Hilliard [7], [6], [8]. More recent works from the 80s and 90s are on the phase-field approach to Ostwald ripening, by Küpper and Masbaum [19]. Multi-particle diffusion models were derived by Voorhees and Glicksman [27], [28]. A stochastic approach is reported by Bhakta and Ruckenstein [1].

(5.2.4) We also mention that an alternative way to derive the system (32)–(34) is to consider the chemical potential:

$$\mu = \frac{\delta E_\epsilon(c)}{\delta c}, \tag{35}$$

and Fick's first law:

$$\mathbf{J} = -D\nabla\mu \tag{36}$$

followed by mass conservation:

$$c_t + \nabla \cdot \mathbf{J} = 0. \tag{37}$$

## 5.3 Numerical Treatment and Results

(5.3.1) The usual model consists of choosing a double-well potential $f(c)$ which includes descriptions of the molar mixing entropy, a mobility factor $M$, and a small parameter of miscibility gap $\gamma$. Although realistic values for $M$ and $\gamma$ can be found, only a biased logarithmic potential can be suggested of the form:

$$f \approx R_g T((1+c)\ln(1+c)+(1-c)\ln(1-c))+\Delta H^0 c(1-c)+\mu_A(1+c)+\mu_B(1-c), \tag{38}$$

(see Küpper and Masbaum [19]) where the first group of terms describe the molar mixing entropy, and the second group accounts for the assymetries. In (38) $R_g$ is the gas constant, $T$ is the absolute temperature, $\Delta H^0$ represents the model of regular solution, and $\mu_A$ and $\mu_B$ are the free energies of the pure phases.

(5.3.2) However, the form (38) for $f$ was found to be rather too complicated and an expensive function to repeatedly evaluate. Instead, the following is a much simpler approach: rather than particle growth, here we only focus on Ostwald Ripening. We use the relatively simple Ginzburg-Landau double-well potential:

$$f(c) = \frac{1}{4}(c^2-1)^2, \tag{39}$$

which has two minima, at $c = -1$ and $c = 1$. These minima represent vapour and condensate, respectively. We take the interval for $x$ as $\Omega = (-1, 1)$ and set $D = 1$. We write the boundary conditions and the system (33)–(34) as

$$\begin{aligned} u &= c_{xx}, \\ c_t &= (f'(c) - \epsilon u_{xx})_{xx}, \\ c_x(\pm 1, t) &= u_x(\pm 1, t) = 0, \qquad \text{for } t > 0 \\ c(x, 0) &= c_0(x). \end{aligned} \tag{40}$$

We spatially discretize the system (40) using centred-difference approximations to the second-order derivatives. We obtain an ODE system with respect to time. To solve this system we use the MATLAB stiff solver Ode15s. We fix the constant $\epsilon = O(10^{-2})$. Under the boundary conditions, it can be easily verified that mass is conserved, and that the energy $E_\epsilon(c)$ in (31) decreases as the evolution takes place.

(5.3.3) In Figure 3 we display the evolution of the phase variable $c(x, t)$ in a binary system (vapour and condensate) with three particles at $t = 0$. We notice that ripening takes place around the larger particle. Figure 4 displays similar phenomena of evolution with five particles at $t = 0$.

(5.3.4) We also observe that the energy (31) decreases while the total mass remains constant, up to the numerical precision which justifies our numerical results.

## 5.4 Comments on Model (iv)

(5.4.1) Cahn-Hilliard modelling was used to describe Ostwald Ripening, in 1-D space & time.

(5.4.2) The potential function $f$ can be found with further work.

(5.4.3) Bi-modal particle size distribution (PSD) is not captured.

(5.4.4) **Modified Phase-Field Modelling:** Bimodal particle-size distribution was explained by a phase-field model which takes nucleation (supercooling) into account. See Wen *et al.* [30]. Find the right free energy function, model the dependence on temperature and investigate the processes of "soft impingement". See Wen *et al.* [30]. Consider some effects similar to the nucleation process.

# 6 Conclusions

## 6.1 Points to Take Further

(6.1.1) There are several approaches to modelling powder ageing. We recommend the following lines of research be followed up:

(6.1.2) Fundamental models: Hints at the relative importance of different physical influences, and separation of time scales, but what are the particle sizes and shapes?

(6.1.3) Some further examinations and interpretations of the data are needed. In Figure 1 (left) the first bump of the "bi-modal" distribution, given the sizes involved, looks as though it contains only about 0.15% of the mass. There are also possibly lower humps to the right – making the distribution (at least) tri-modal. The scale is logarithmic so these could contain more mass, given the relevant length scales, than the pronounced left-hand bump. Within the first 30 minutes, Figure 1 (left) shows a shift of the main hump to the right, corresponding to a doubling of the particle size. Figure 1 (right) only indicates a reduction of about 20% (not 50%) in SSA during that time.

(6.1.4) Discrete and continuum models for particle sizes: Model (ii) has nice time-dependent equations, that can capture bimodal particle size distributions. But what is the physical justification? Can we choose realistic rate constants?

(6.1.5) In the continuum Model (iii) the work may help interpret the dynamical systems Model (ii) when the number of particle sizes $N$ is realistically

large but also uncomputable. In Model (iii) are we considering the right scaling regime, or will $\hat{m} \gg \hat{c}$ need investigation?

(6.1.6) In Model (iv), the Cahn-Hilliard eqs, can capture spatial interactions, but how do we get bimodal size distributions? Can Model (iv) help inform the choices of rate constants in Models (ii) and (iii)?

(6.1.7) Overall, in the basic science and in the mathematical modelling, there are many challenges and useful prospectives lines of research in powder ageing. While some progress has been made during the study group, there is much left to be understood and modelled in detail.

# 7 Bibliographical Note:

The following references are not cited in the report above, but were used during ESGI-85 and are listed in the bibliography: These are the papers of Brown *et al.* [2], Burnham *et al.* [3], [4], [5], Edmunds *et al.* [11], Fischmeister and Arzt [15], Gee *et al.* [16], Gershanik and Zeini [17], Hirata *et al.* [18], Maiti and Gee [21], [22], Monroe *et al.* [23], Pitchimani *et al.* [24], Sinka [26] and Zapeda *et al.* [32].

# Bibliography

[1] A. Bhakta and E. Ruckenstein. Ostwald ripening – a stochastic approach. *J. Chem. Phys.*, 103(16):7120–7135, 1995, doi: 10.1063/1.470341.

[2] G.W. Brown, M.D. Sandstrom, A.M. Giambra, J.G. Archuleta, and D.C. Monroe. Thermal analysis of pentaerythritol tetranitrate and development of a powder aging model. *37th Annual Conference of the North American Thermal Analysis Society, Lubbock, TX, USA, LA-UR-09-05019*, 1:1–12, 2009.

[3] A.K. Burnham. An nth-order Gauss energy distribution model for sintering. *Chemical Engineering Journal*, UCRL-JRNL-206339:1–9, 2004.

[4] A.K. Burnham, R. Gee, A. Maiti, R. Qui, P. Rajasekar, B. Weeks, and L. Zepeda-Ruiz. Experimental and modeling characterization of petn mobilization mechanisms during recrystallization at ambient conditions. *UCRL-TR-216963, Lawrence Livermore National Laboratory, USA*, pages 1–21, 2005.

[5] A.K. Burnham, G.E. Overturf II, R. Gee, P. Lewis, R. Qui, D. Phillips, B. Weeks, R. Pitchimani, A. Maiti, L. Zepeda-Ruiz, and C. Hrousis. Progress towards a petn lifetime prediction model. *27th Aging, Compatibility and Stockpile Stewardship Conference Los Alamos, NM, USA*, pages 1–5, 2006.

[6] J.W. Cahn. Free energy of a nonuniform system. 2. Thermodynamic basis. *J. Chem. Phys.*, 30(5):1121–1124, 1959, doi: 10.1063/1.1730145.

[7] J.W. Cahn and J.E. Hilliard. Free energy of a nonuniform system. 1. Interfacial energy. *J. Chem. Phys.*, 28(2):258–269, 1958, doi: 10.1063/1.1744102.

[8] J.W. Cahn and J.E. Hilliard. Free energy of a nonuniform system. 3. Nucleation in a 2-component incompressible fluid. *J. Chem. Phys.*, 31(3):688–699, 1959, doi: 10.1063/1.1730447.

[9] C. Cowan. The cahn-hilliard equation as a gradient flow. *MS thesis, Simon Frazer University, Canada*, 2005.

[10] J. Crank. *The Mathematics of Diffusion.* Clarendon Press, Oxford, 1979.

[11] E. Edmonds, A. Hazelwood, T. Lilly, and J. Mansell. Densification of powders by particle deformation. *Powder Metallurgy*, 174:42–45, 2007.

[12] M. Eisenmann. *Porous Powder Metal Technology: Year 2000 ASM Handbook*, volume 7. ASM Internationals USA, 2000.

[13] C.M. Elliott. Numerical studies of the Cahn-Hilliard equation for phase separation. *IMA Journal of Appl. Math.*, 38:97–128, 1987.

[14] M.M. Faktor and I. Garrett. *Growth of Crystals from the Vapour.* Chapman and Hall, 1974.

[15] H.F. Fischmeister and E. Arzt. Development of in-situ surface area analysis for detonators. *Powder Technology*, 26:82–88, 1983.

[16] R. Gee, C. Wu, and A. Maiti. A course-grained model for petn crystals. *Applied Physics Letters*, 21907(1):1–13, 2006.

[17] A.P. Gershanik and Y. Zeiri. Sublimation rate of energetic materials in air: Rdx and petn. *Propellants Explosives Pyrotechnics*, 37:207–214, 2012.

[18] Y. Hirata, A. Hara, and I.A. Aksay. Thermodynamics of densification of powder compact. *Ceramics International*, 35:2667–2674, 2009, doi: 10.1016/j.ceramint.2009.03.006.

[19] T. Küpper and N. Masbaum. Simulation of particle growth and Ostwald ripening via the Cahn-Hilliard equation. *Acta Metallurgica et Materialia*, 42(6):1847–1858, 1994, doi: 10.1016/0956-7151(94)90010-8.

[20] I.M. Lifshitz and V.V. Slyozov. The kinetics of precipitation from supersaturated solid solutions. *J. Phys and Chem. of Solids*, 19(1–2):35–50, 1961, doi: 10.1016/0022-3697(61)90054-3.

[21] A. Maiti and R.H. Gee. Modeling growth, surface kinetics, and morphology evolution in petn. *Propellants Explos. Pyrotech.*, 34:489–497, 2009.

[22] A. Maiti and R.H. Gee. Petn coarsening – predictions from accelerated aging data. *Propellants Explos. Pyrotech.*, 36:125–130, 2011, doi: 10.1002/prep.201000106.

[23] D.C. Monroe, K.E. Laintz, J.F. Kramer, and P. Peterson. Petn: Variation in physical and chemical characteristics related to aging. *Energetic Material: Insensitivity, Aging, Monitoring 37th Intl. Conf. of ICT, Karlsruhe, Germany. LA-UR-06-2633*, pages 1–7, 2005.

[24] R. Pitchimani, W. Zheng, S. Simon, L. Hope-Weeks, A.K. Burnham, and B.L. Weeks. Thermodynamic analysis of pure and impurity doped pentaerythritol tetranitrate crystals grown at room temperature. *NATAS 34th Annual conference Bowling Green, KY, USA*, pages 1–6, 2006.

[25] L. Ratke and P.W. Voorhhes. *Growth and Coarsening: Ostwald Ripening in Material Processing*. Springer, 2002.

[26] L.C. Sinka. Modelling powder compaction. *KONA*, 25:4–22, 2007.

[27] P.W. Voorhees and M.E. Glicksman. Solution to the multi-particle diffusion problem with applications to Ostwald ripening. 1. Theory. *Acta Metallurgica*, 32(11):2001–2011, 1984, doi: 10.1016/0001-6160(84)90180-9.

[28] P.W. Voorhees and M.E. Glicksman. Solution to the multi-particle diffusion problem with applications to Ostwald ripening. 2. Computer simulations. *Acta Metallurgica*, 32(11):2013–2030, 1984, doi: 10.1016/0001-6160(84)90181-0.

[29] C. Wagner. *Z. Elektrochem*, 65:581–581, 1961.

[30] Y.H Wen, J.P. Simmons, C. Shen, C. Woodward, and Y. Wang. Phase-field modeling of bimodal particle size distributions during continuous cooling. *Acta Materialia*, 51(4):1123–1132, 2003.

[31] J.H. Yao, K.R. Elder, H. Guo, and M. Grant. Theory and simulation of Ostwald ripening. *Phys. Rev. B*, 47(21):14110–14125, 1993.

[32] L.A. Zapeda-Ruiz, A. Maiti, R. Gee, G.H. Gilmer, and B. Weeks. Size and habit evolution of petn crystals – a lattice Monte Carlo study. *J. Crystal Growth*, 25(UCRL-JRNL-219543):1–22, 2006.

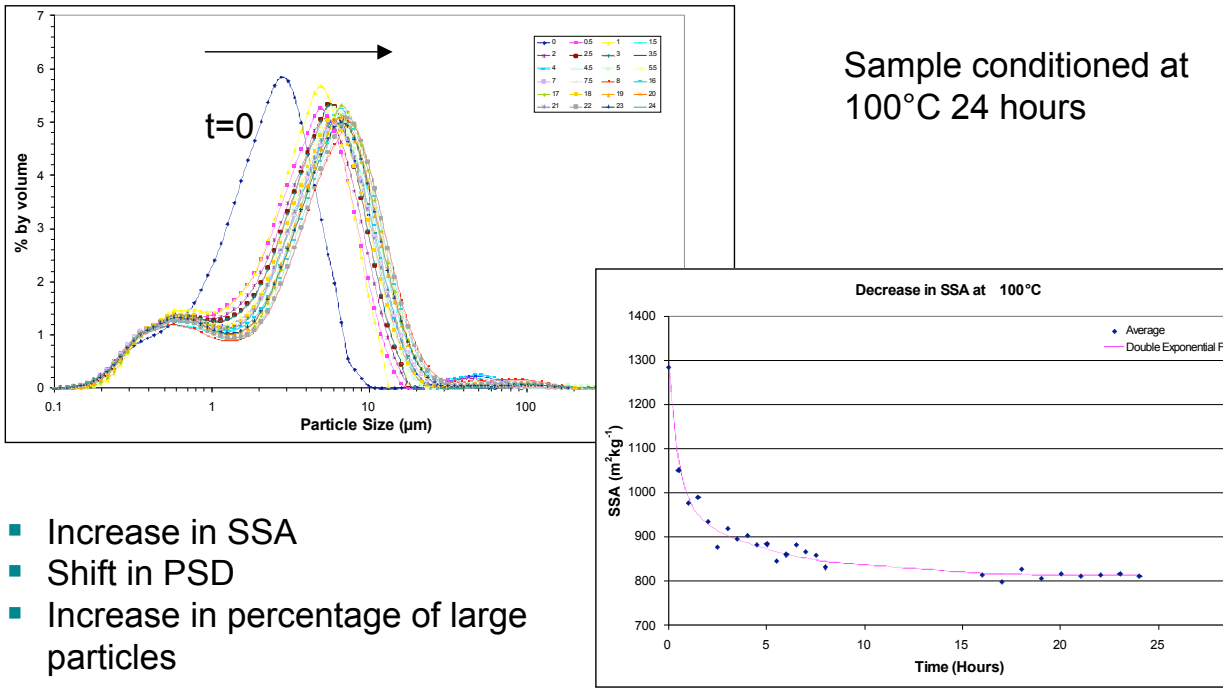


**Figure 1:** Left-hand plot: measured particle size distribution (PSD) and its change over time. Right-hand plot: measured specific surface area (SSA) as a function of time. [Reproduced courtesy of AWE Ltd.]

bimodal.jpg 806×806 pixels 20/06/2012 16:31

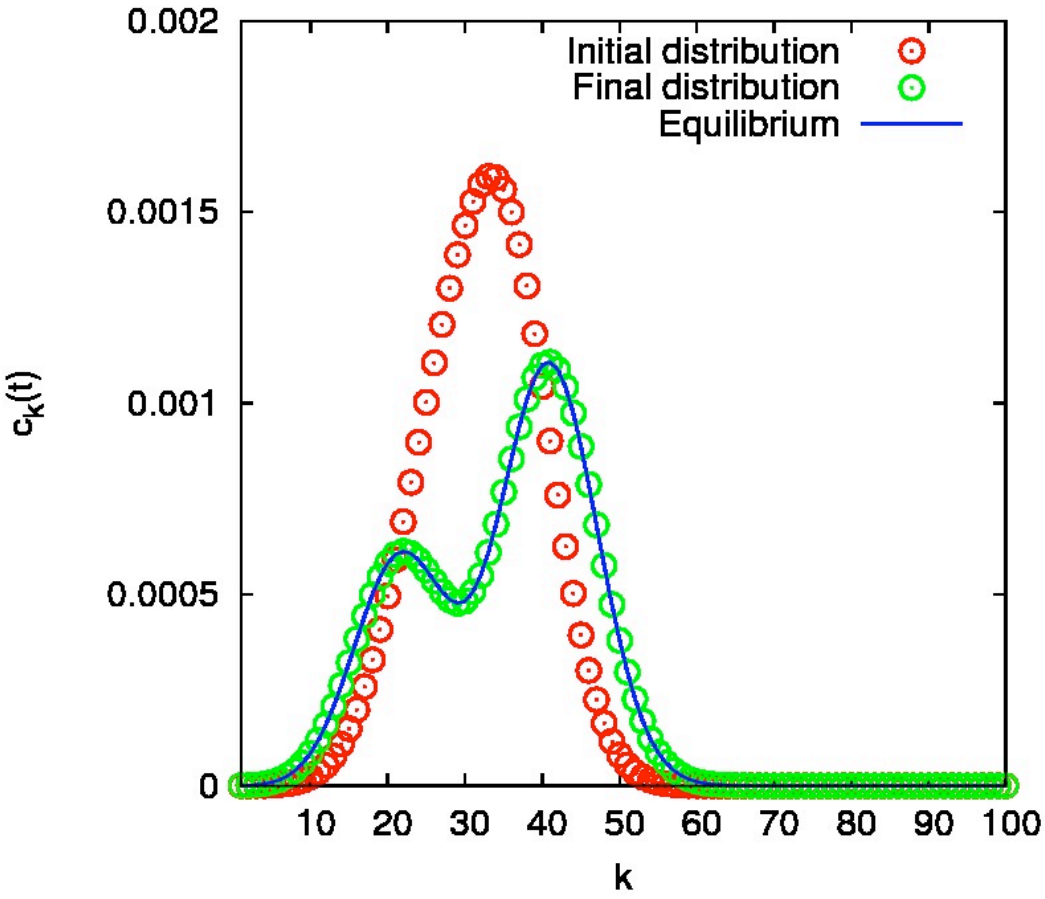


**Figure 2:** Chemical kinetics Model (ii): results for PSD, $c_k$, as a function of particle size, $k$. Unimodal initial data (red dots) evolves over time to a bimodal distribution (green dots). The latter are seen to sit on the long-time equilibrium distribution (blue curve).

lambdak.jpg 806×806 pixels 20/06/2012 16:47

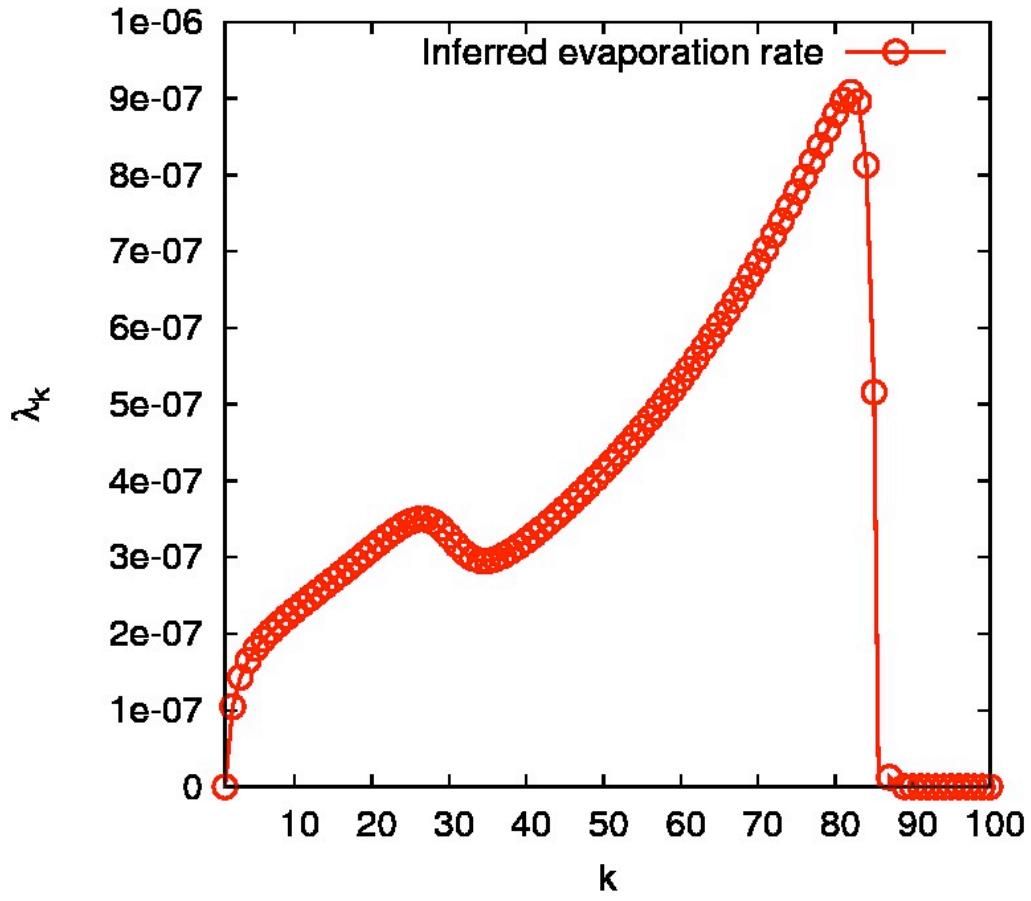


**Figure 3:** Chemical kinetics Model (ii): inferences from equilibrium state: evaporation rates $\lambda_k$, for fixed condensation rate $\gamma$ independent of $k$.

SSA.jpg 806×806 pixels 20/06/2012 16:49

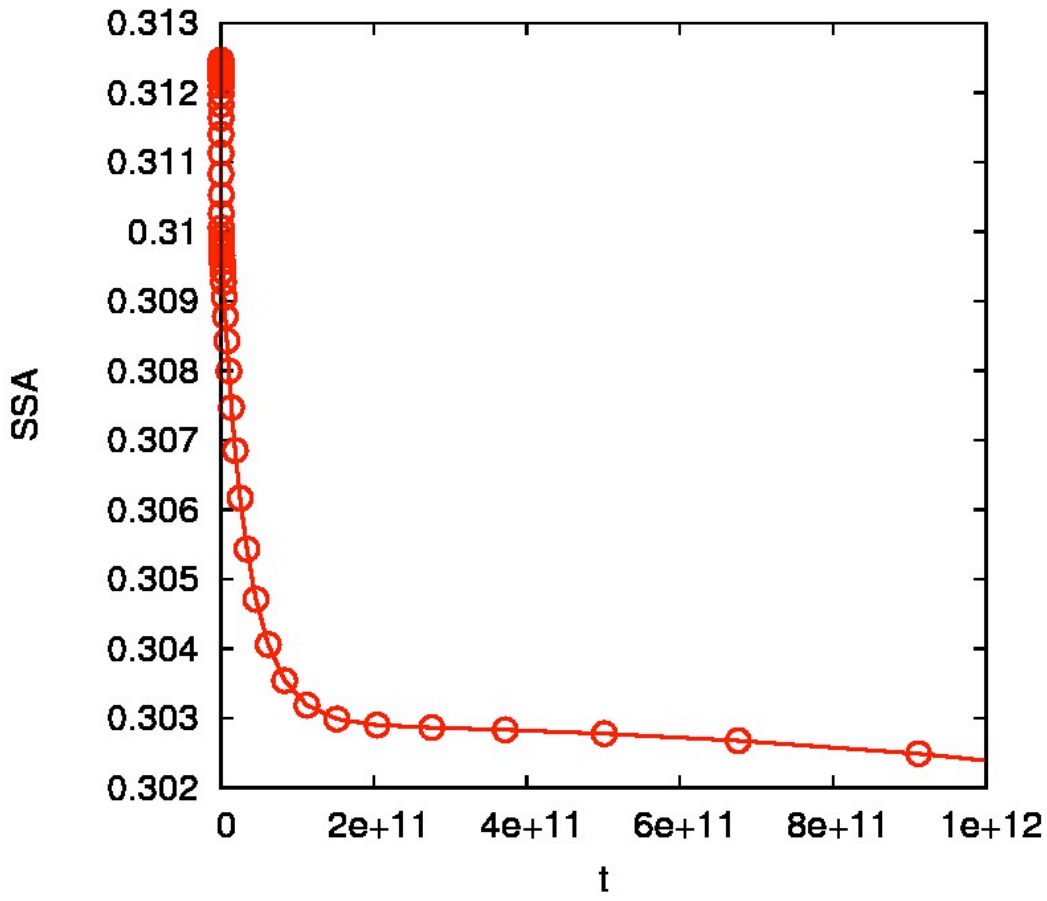


**Figure 4:** Chemical kinetics Model (ii): results for SSA as a function of time. Compare with Figure 1 (right).

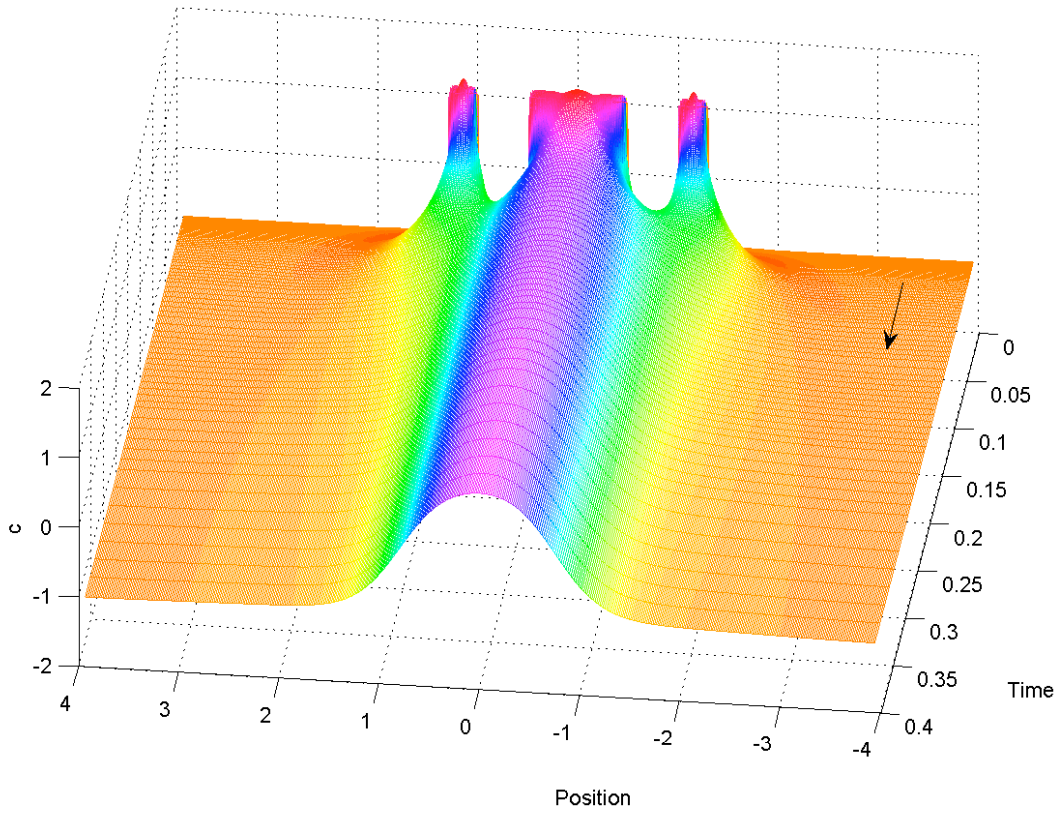


**Figure 5:** Cahn-Hilliard Model (iv): Ripening in a binary system with initially three particles of varying sizes. The arrow points in the direction of increasing time. The colours label the different levels of the phase variable $c$, from $c = -1$ (vapour) up to $c = +1$ (solid).

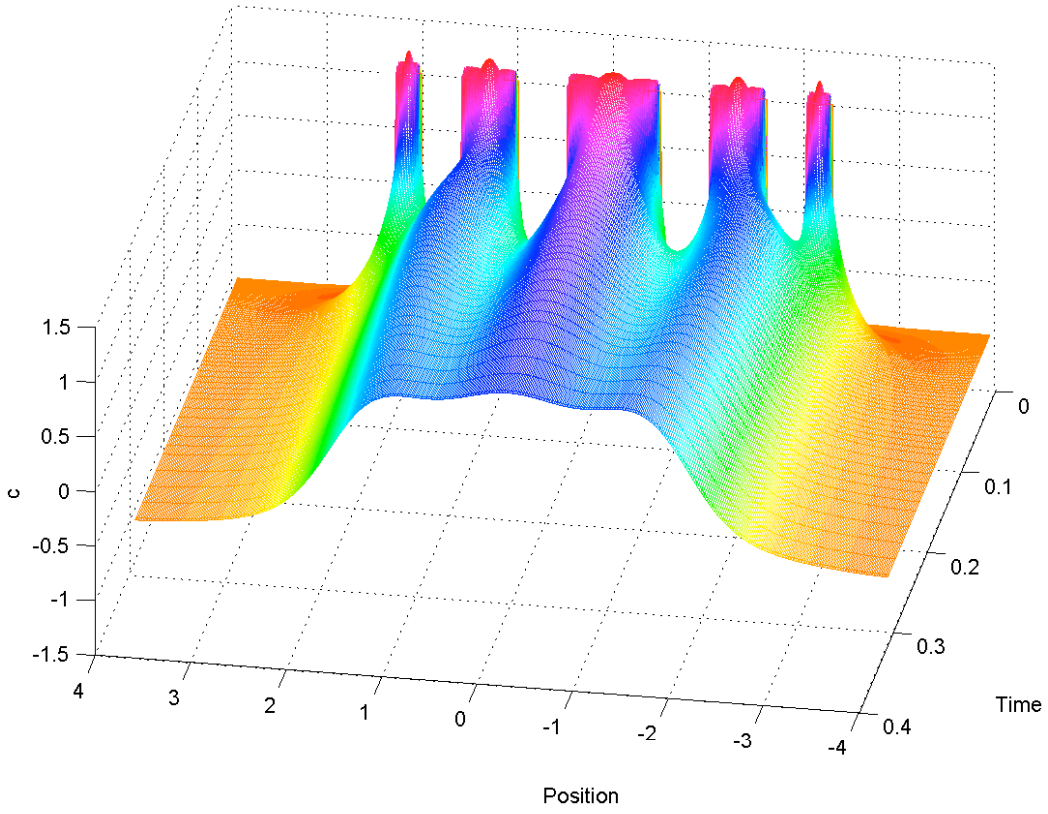


**Figure 6:** Cahn-Hilliard Model (iv): Ripening in a binary system with initially five particles of varying sizes. The colours label the different levels of the phase variable $c$, from $c = -1$ (vapour) up to $c = +1$ (solid)